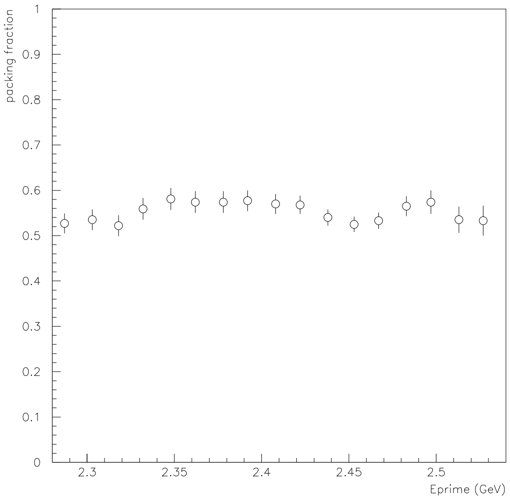

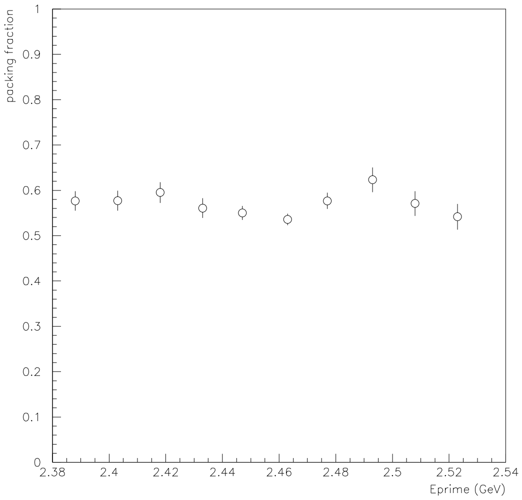

Figure 7.14: $^{15}ND_3$ (left) and $^{15}NH_3$ (right) packing fractions as a function of E′. The $^{15}ND_3$ data is from the set of runs 22199-22213. The $^{15}NH_3$ packing fraction is from all 22 proton runs.

7.7 $^{15}NH_3$ Packing Fractions

Packing fractions for the proton targets were calculated in a similar fashion. More attention to the details of the model was necessary due to the sharp elastic proton peak. Errors introduced into the model of the cross section as a function of scattering energy or angle, or mistreatment of radiative corrections could result in large deviations from the data. Including a large angular range is also more difficult with the $^{15}NH_3$ target. The sharp elastic peak at the central angle was broadened in E' as the elastic peak falls at different scattered energies for different scattering angles. The model had to have the appropriate angular dependence in order to match the data. The model was calculated for all θ bins across the angular range of the data used for packing fraction determination (nominally $\pm$ 0.5° from the central angle of 15.72°). For completeness and consistency, the calculation of the modelled rates was calculated over all θ bins for all materials in the $^{15}NH_3$ target.

Table 7.6 lists the packing fraction values for $^{15}NH_3$ run groupings. Proton packing fractions were consistent over all run periods, and all packing fraction values for